Influence of the mechanical properties of the necrotic core on the growth and remodelling of tumour spheroids

Influence of the mechanical properties of the necrotic core on the growth and remodelling of tumour spheroids.

Chiara Giverso*[a], Luigi Preziosi[a]

[a]*Dept. of Mathematical Sciences, Politecnico di Torino, Corso Duca degli Abruzzi 24, 10129 Torino, Italy*

Abstract

Multicellular tumour spheroids (MCTSs) are complex biological materials, undergoing both growth, due to cell proliferation, and remodelling, thanks to the ability of cells to reorganize the bonds among them. In this paper, we study the mechanical behaviour of MCTSs, treated as porous materials, composed of cells and filled with water, and we use the notion of evolving natural configurations to incorporate cells' capability to reorganize and proliferate. We model the MCTS as possibly made up of three concentric layers: the necrotic core, either calcified of filled by liquid, the quiescent region, composed by cells that are alive but not dividing and the outermost proliferative ring. The resulting system of equations is used to simulate the response of a quiescent tumour spheroid when an external load is applied and the proliferation of a MCTS in response to nutrients, either when the aggregate is let free to expand or when it is compressed by the external environment. The results show the importance of remodelling on the capability of cells to redistribute inside the living structure and the influence of the mechanical properties of the inner necrotic structure, when its size is relevant.

Keywords: growth and remodelling, multicellular tumour spheroid, necrotic core, evolving natural configurations

1. Introduction

The formulation of a mathematical model able to simulate the process of cell growth in vitro and in vivo is of great interest both from the biological and the mathematical point of view. Indeed, modelling the proliferation of tumours has the potential of shedding light on the interactions among the biological mechanisms involved in the process, becoming a useful tool in cancer research, possibly improving diagnostic treatments.

Solid tumours develop initially as a single undifferentiated mass of abnormal cells, that proliferate more rapidly than the healthy cells around them. In this very first stage, tumour growth is not associated with the formation of new blood vessels (avascular phase) and thus cells receive their nutrient supply by diffusion from the existing vasculature [65]. Imaging techniques and biological tests through isolation and staining [56] showed that, as the tumour size increases (up to hundreds of μm), cells at the interior become quiescent, i.e., they are not dividing but are alive. Then, the avascular mass continues to grow until cell close to the centre, being deprived of vital nutrients, die forming the central necrotic core [20, 56]. Therefore, avascular multicellular tumour spheroids (MCTSs), with dimensions up to several millimetres in diameter, are typically composed by an inner necrotic core, surrounded by a shell of quiescent cells, and an outermost thin layer of live, proliferating cells [20].

The boundaries between the different layers inside a multicellular spheroid may vary in time, because quiescent cells can start dividing again if environmental conditions change and conversely proliferating cells might turn quiescent. At the same time, a portion of the quiescent region can undergo both apoptosis and

*Corresponding author

Email address: chiara.giverso@polito.it (Chiara Giverso*)

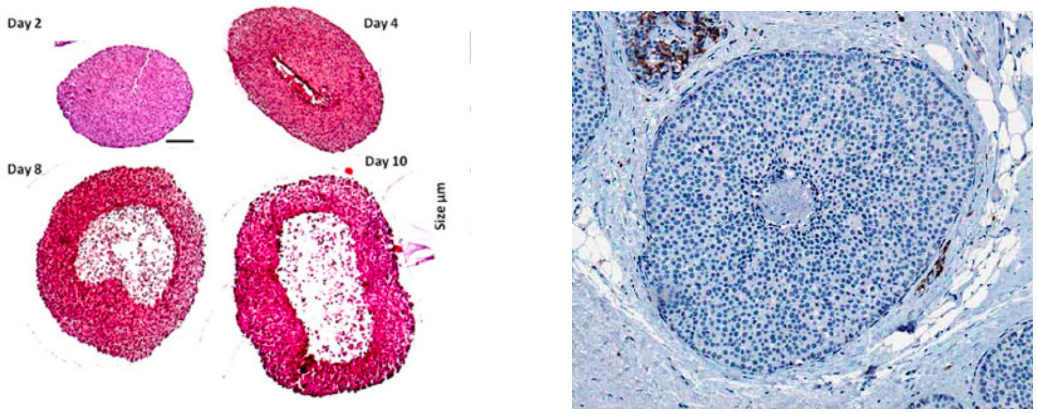

(a) (b)

Figure 1: Morphology of multicellular tumour spheroids. (a) A human melanoma MCTS after 2, 4, 8 and 10 days in culture (scale bar = 100 μm) (taken with permission from [52]: the liquid necrotic core start to form after 2 days. (b) Lobular carcinoma in situ (LCIS) with a necrotic calcified core (taken with permission from [46]).

necrosis, enlarging the necrotic core. In contrast to apoptosis, which is the naturally occurring programmed cell death, necrosis results in the premature death of cells and it is caused by external factors (e.g. nutrient deprivation, infections, hypoxia, presence of tumour necrosis factor...) [29, 34, 35]. Thus, apoptotic cells appear sporadically as isolated, shrunken cells, and are generally soon replaced by either proliferative or quiescent cells, whereas necrotic cancer cells form large contiguous regions (such as the necrotic cores in a MCTS) where oxygen, glucose or eventually other growth factors are too low to sustain cell survival [34, 35]. Necrosis starts with a rapid swelling by osmosis up to several times the initial cell volume and subsequent lyses with leaks of fluids and other proteins [34, 35]. In some cases, the necrotic cells undergo dissolution and are removed from the system entirely, leading to the formation of an inner cavity filled with liquid and eventually some necrotic debris (see Fig. 1-a), while, in other cases, the necrotic core is separated from the rest of the tumour, so that the clearance of the necrotic material is prevented and the whole region undergoes dystrophic calcification (see Fig. 1-b) [15, 35, 36]. Calcification has been detected in many cancers, such as in breast cancer and in particular ductal carcinoma in situ (DCIS) [41, 68], in glioblastoma multiforme [45], in colorectal and ovarian cancer [15, 53] and in a wide variety of epithelial, mesenchymal, lymphoid, or germ cell neoplasms [15]. However the pathophysiology of calcification in primary and metastatic malignancies is extremely heterogeneous and not completely understood [15].

Since the very early stages of tumour progression are rarely seen clinically because of the small size of the cell masses and the absence of symptoms, the initial avascular growth phase and the different regions composing the MCTS can be easily studied in vitro, by culturing cancer cells in the form of three dimensional spheroids in a liquid medium or gel containing appropriate nutrients [19, 44]. This assay, introduced by Sutherland and coworkers in the early 1970s [59, 60], has been extensively used to study the properties of tumours and its internal architecture, to investigate subsequent stages of cancer progression, and to predict the response to therapeutic treatments, because it possesses growth kinetics which are very similar to the one shown by tumour masses in vivo [66] (see [30, 37] for reviews). The relative abundance of in vitro studies on MCTSs [19, 21, 29, 34, 60, 61, 66] has also fostered the development of several mathematical models [2, 8, 10, 17, 25, 40, 42, 43, 49, 55, 63, 67]. Without claiming to be exhaustive, since the literature on the growth of cellular aggregates is so widespread, we will focus only on those contributions that are fundamental for this work, referring the interested reader to [4, 5, 40, 49, 64] for a detailed review on mathematical modelling of solid tumour growth.

Typically, mathematical models of MCTSs in the literature treat the tumour as a spherical mass of cancer cells which grows in response to an external nutrient supply. The layer of proliferating cells surrounds a region containing non-proliferating, quiescent cells [7] and, eventually, a central necrotic core [10, 8]. The resulting

system of equations comprise one or eventually more ordinary differential equations, derived from mass conservation applied to the whole tumour and possibly the different subregions, and at least one reaction-diffusion equation describing the distribution within the tumour of the chemicals (e.g., oxygen, glucose, growth inhibitory factors, ...) [10, 40, 49]. All these works consider the tumour mass as composed only by cells that can proliferate or die or eventually stay at rest. However multicellular aggregates are complex living materials, composed by different types of cells, with water filling the interstitial space. In particular, the introduction of the liquid phase is fundamental in order to properly describe the flow of nutrients inside multicellular spheroids, thus a multiphase framework would be more adapt to describe the whole process. The description of solid tumours as a multiphasic mixtures date back to the late-1990s [47, 48] and in the last years several multiphase models, with either sharp or diffuse interface separating the tumour from the healthy tissue and eventually the different layers in the aggregate, have been developed and applied with success to describe tumour growth [16, 17, 43, 49, 55, 67]. However in the aforementioned multiphase models, the mechanical response to stress of necrotic cells is not distinguished from the one of live and quiescent cells. Indeed necrotic cells are hinted in the source/sink term, without explicitly accounting for the additional interface between living and dead cells and without considering the different mechanical properties of the necrotic region from the rest of the MCTS. Furthermore, none of these multiphase continuous models have examined the possible calcification of necrotic debris, which dramatically change the mechanical response of that portion of tissue. Some efforts to characterize the necrotic core biomechanical properties and include calcifications have been done, for instance, in the multiscale agent-based cell model proposed in [41], but, also in this case, the potential impact of the necrotic core on tumour progression and on the ability to sustain external stress is missed. However, it is well known that necrosis plays a prominent role in many carcinomas and the mechanical characteristic of the necrotic core can alter the response of tumour spheroid to external stresses [58].

Therefore, in the present paper, considering the tumour composed by cells living in a watery gel full of nutrients and using the tools provided by mixture theory, we formulate a mathematical model to represent the growth and remodelling of a multicellular spheroid under the application of an external load, that represents the stress exerted by either the medium in which the tumour spheroids are cultured or, eventually, the healthy tissue. In order to encapsulate in the model growth and cells reorganization which inexorably occurs inside living systems, we use the theory of material with natural evolving configurations [32, 33, 54]. In particular, the proposed model follows the work done by Ambrosi and Mollica [1, 2], in which the response of tumour spheroids undergoing growth is studied, and by Preziosi and Ambrosi [3, 50] in which the role of remodelling in tumour response is introduced. In particular, in [1, 2], spheroids are considered as a monophasic elastic material, undergoing growth depending on the external loading and the availability of nutrients, without considering the role of remodelling, whereas in [23, 24, 50] a remodelling equation is introduced, but the process of growth inside spheroidal aggregates is not exploited. In [3] a similar model, with different remodelling equation, is presented and applied to the description of tumour growth inside a cylindrical duct (with rigid wall). Moreover, in these works the diffusion and transport of nutrients are not exploited. Nutrient availability controls the duplication of cells and its depletion limits the expansion of the tumour spheroids and defines the presence of the quiescent and necrotic region.

Therefore, in the present work, we first consider a simple setting, composed of a necrotic core and a quiescent ring, undergoing radial compression, then we consider the interplay between growth and remodelling in a tumour composed of a necrotic core, a quiescent and a proliferative ring, determined by the availability of nutrients in the external environment. In both conditions, we consider the cases in which the central necrotic core is composed either by calcified debris resulting from the death of cells (i.e., calcified necrotic core) or the case in which debris have been removed and the spheroid is left with a cavity filled by water (i.e. liquid necrotic core).

The paper is structured as follows: Section 2 is devoted to the derivation of the equations describing the growth and remodelling of a tumour spheroid in vitro. The balance laws and constitutive equations presented in Section 2.1 are then set in spherical coordinates (see Section 2.2). Results are presented in Section 3, considering the pure remodelling of a spheroid under an external load, and the growth and remodelling of a MCTS composed by necrotic, quiescent and proliferative regions and considering the influence of the

mechanical properties of the central necrotic core on the ability to sustain internal and external stresses. Finally, the main outcomes of this work and future development are discussed in Section 4.

2. Mathematical Model

The mathematical model presented below describes the evolution of a multicellular tumour spheroid growing in response to an externally-supplied nutrient, such as oxygen or glucose. We assume that the tumour is radially-symmetric over the whole process and that contains proliferating, quiescent and necrotic cells. The proportion of quiescent and proliferating cells changes as the tumour grows, whereas the size of the calcified core is fixed, since we assumed that the necrotic process occurs over longer times than the ones considered in the present work [41]. Indeed, it has been estimated that while the cell swelling and lysis, associated to apoptosis and to the very first stage of necrosis, occur in some hours, calcification takes 15-20 days [41] to establish.
In particular, we modelled the multicellular tumour spheroid as a porous medium composed of a "solid" fraction, ϕ_s, representing cells, and a liquid phase, ϕ_ℓ, representing the interstitial fluid and we assume that the saturation condition for the aggregate is $\phi_s+\phi_\ell = \phi_{max}$, where ϕ_{max} is a given constant, possibly, but not necessarily, equal to one. We, then, consider the velocities $\boldsymbol{v}_s$ of the solid phase and $\boldsymbol{v}_\ell$ of the liquid phase. In order to properly describe the growth and remodelling processes occurring inside the living structure, we refer to the theory of material with evolving natural configurations [32, 33, 54] and we introduce the second-order tensors $\mathbf{F}_g$ which represents pure growth/death (therefore accompanied with cell mass variation), $\mathbf{F}_p$ which describe the anelastic deformation due to the rearrangements among cells (i.e. remodelling) and $\mathbf{F}_n$ which represent the stress-induced deformation. Referring to Fig. 2, the tensor $\mathbf{F}_g$ maps vectors attached to $\mathscr{B}_r$, which is the *reference configuration* into vectors attached to what is generally called *grown configuration* $\mathscr{B}_g$, whereas the tensor $\mathbf{F}_p$ maps vectors attached to $\mathscr{B}_g$ into vectors attached to a locally relaxed configuration, which is often referred to as *natural configuration* [51] and denoted by $\mathscr{B}_n$. Therefore, using the multiplicative decomposition [39], the tensor $\mathbf{F}$ is decomposed as $\mathbf{F} = \mathbf{F}_n\mathbf{F}_p\mathbf{F}_g$. The variations of volume of the solid phase due to the deformation when no growth and remodelling take place is denoted by $J_n = \det(\mathbf{F}_n)$, whereas the volume increase due to growth is represented by $J_g = \det(\mathbf{F}_g)$. We assume that deformations due to remodelling takes place, without changes in volume, i.e. $J_p = \det(\mathbf{F}_p) = 1$, so that the multiplicative decomposition of $\mathbf{F}$ implies $J = J_nJ_pJ_g = J_nJ_g$.

2.1. Balance laws

For a closed saturated biphasic mixture, composed by incompressible solid and liquid phases (i.e. the true densities of the solid and liquid phases, i.e., $\hat{\varrho}_s = \rho_s/\phi_s$ and $\hat{\varrho}_\ell = \rho_\ell/\phi_\ell$, are constant), the balance laws in the Lagrangian form, referring to the solid constituent (in order to have all the quantities expressed in the reference configuration which is fixed in time) [27], assuming that $\hat{\rho}_s = \hat{\rho}_\ell$ (which is reasonable being cells mainly composed of water), read

$$\dot{\overline{(J\phi_s)}} = J\phi_s\Gamma_s, \tag{1}$$

$$\dot{J} + \mathrm{Div}\left(J\phi_\ell\mathbf{F}^{-1}(\boldsymbol{v}_\ell - \boldsymbol{v}_s)\right) = 0, \tag{2}$$

where the operator $\mathrm{Div}(\cdot)$ is the divergence computed with respect to the material coordinates. Since $J_g = J/J_n = J\phi_s/\phi_{sn}$,

$$\phi_s = \frac{\phi_{sn}}{J_n} = \phi_{sn}\frac{J_g}{J}. \tag{3}$$

and the volumetric fraction of the solid phase, ϕ_s, is determined once the volumetric deformations J and J_g are known and the constant solid volumetric fraction ϕ_{sn} 'seen' from the natural configuration is assigned. Together with mass balance, also the balances of momentum of the cellular and liquid phase have to be provided. We accept the validity of Darcy's law, so that the fluid flow depends on the permeability of the medium ($\mathbf{K}$) and on the interstitial pressure (p) gradient

$$\nu\phi_\ell(\boldsymbol{v}_\ell - \boldsymbol{v}_s) = -\mathbf{K}\,\mathrm{grad}(p), \tag{4}$$

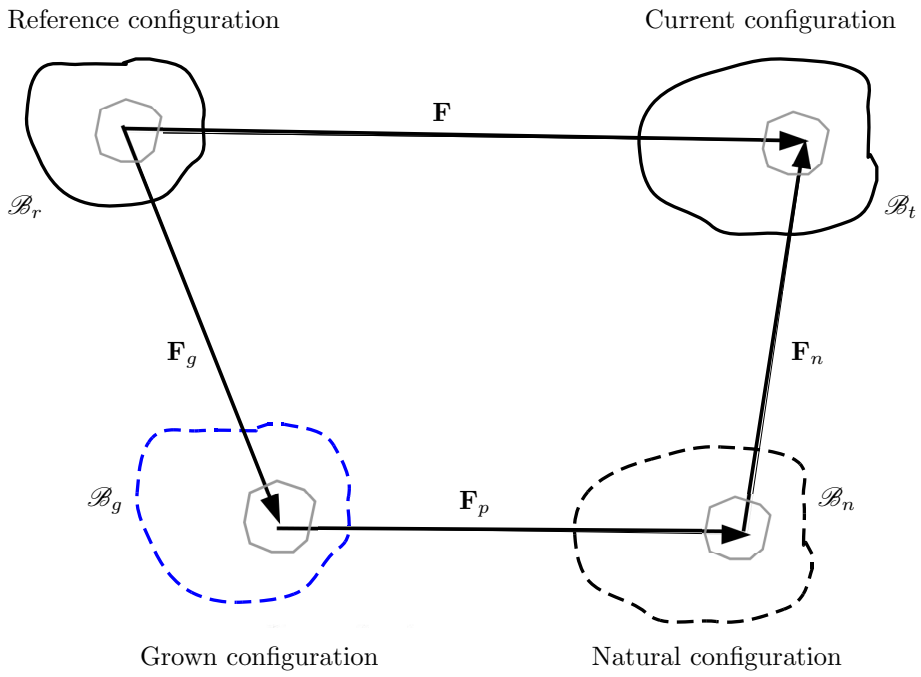

Figure 2: Diagram of the states from the original unstressed configuration $\mathcal{B}_r$ to the current configuration $\mathcal{B}_t$, in the framework of multiple natural configurations. $\mathbf{F}_n$ identifies the deformation without anelastic deformations, $\mathbf{F}_p$ describes the reorganization of cells inside the aggregate and $\mathbf{F}_g$ the anelastic deformation due to growth/death.

where ν is the viscosity of the fluid phase. Substitution of this result into (2) yields

$$\dot{J} = \frac{1}{\nu}\mathrm{Div}\left(J\mathbf{F}^{-1}\mathbf{K}\mathbf{F}^{-T}\,\mathrm{Grad}(p)\right), \tag{5}$$

where we wrote the pressure gradient in material coordinates, i.e. $\mathrm{grad}(p) = \mathbf{F}^{-T}\mathrm{Grad}(p)$.
Assuming that the external body force density is null, the material, local form of the momentum balance law for the mixture, written with respect to the reference placement $\mathscr{B}_r$ and neglecting inertial term, is given by

$$\mathrm{Div}(\mathbf{P}) = \mathbf{0}, \tag{6}$$

where $\mathbf{P}$ is the first Piola-Kirchhoff stress tensor of the mixture, and it can be approximated with the sum of the stress tensors of the solid and liquid phase, $\mathbf{P} = \mathbf{P}_s + \mathbf{P}_\ell$. The tensors $\mathbf{P}_s$ and $\mathbf{P}_\ell$ are defined through the standard Piola transformations

$$\mathbf{P}_s := J\mathbf{T}_s\mathbf{F}^{-T} \tag{7}$$

$$\mathbf{P}_\ell := J\mathbf{T}_\ell\mathbf{F}^{-T}. \tag{8}$$

where $\mathbf{T}_s$ and $\mathbf{T}_\ell$ denote the Cauchy stress tensors of the solid and fluid phase and J and $\mathbf{F}$ refer to the solid phase.
In order to close the mathematical problem resulting from (5) and (6), it is necessary to provide information about the stresses $\mathbf{T}_s$ and $\mathbf{T}_\ell$. The cellular component is assumed to be hyperelastic and isotropic, and it is modelled by a modified Neo-Hookean constitutive equation [3], which leads to the following expressions

$$\mathbf{T}_s = -\phi_s\left(p + \Sigma(\phi_s) + \frac{1}{3}\mu\,\mathrm{tr}\,(\mathbf{B}_n)\right)\mathbf{I} + \mu\phi_s\mathbf{B}_n, \tag{9}$$

where $\mathbf{B}_n = \mathbf{F}_n\mathbf{F}_n^T$ and $\Sigma(\phi_s)$ is a stress function that in the following we will assume to have the form $\Sigma(\phi_s) = E\dfrac{\phi_s - \phi_0}{\phi_{max} - \phi_s}$. The liquid component is assumed to be inviscid, i.e $\mathbf{T}_\ell = -\phi_\ell p$. In the following, we will use the apex $'$ to indicate the deviatoric part of the stress tensor of the solid phase, whereas the apex $*$ stands for the constitutive part, i.e., $\mathbf{T}'_s = \mathbf{T}_s - \frac{1}{3}\mathrm{tr}(\mathbf{T}_s)\mathbf{I}$ and $\mathbf{T}^*_s = \mathbf{T}_s + \phi_s p\mathbf{I}$.
Once it is known how the material behaves from the natural configuration to the actual state, we need to describe how the natural configuration evolves, through remodelling and growth. For the evolution of the internal reorganization, we use the relation introduced in [23], which links the the plastic velocity gradient to the plastic deformation tensor $\mathbf{T}_p = \mathbf{F}_n^T\mathbf{T}'_s\mathbf{F}_n^{-T}$

$$\mathbf{L}_p = \frac{J}{2\eta(\phi_s)}\left[1 - \frac{\tau(\phi_s)}{f(\mathbf{T}'_s)}\right]_+ \mathrm{sym}\left(\mathbf{F}_n^T\mathbf{T}'_s\mathbf{F}_n^{-T}\right), \tag{10}$$

where $[\cdot]_+$ stands for the positive part of its argument. We observe that in (10), the term containing the yield stress switches on just when the stress overcomes the yield stress $\tau(\phi_s)$ in terms of the set frame invariant measure of the stress of the cellular constituent $f(\mathbf{T}'_s)$. In this case the energy is no longer elastically stored but it is spent in cell unbinding and cytoskeleton reorganization at the microscopic scale, which produces the spheroid rearrangement at the macroscopic scale.
Finally, we have to consider the equation representing the growth of the cellular constituent. In [3], it was shown that the evolution of the growth term satisfies

$$\frac{\dot{J}_g}{J_g} = \Gamma_s\,. \tag{11}$$

In this work, we will assume that the duplication of cells and its depletion is limited by contact inhibition and is controlled by nutrient availability, fixing a minimum threshold of nutrients concentration, c_{n0} above which cells can proliferate, so that we can set $\Gamma_s = \gamma_s(\phi_{max} - \phi_s)(c_n - c_{n0})_+$. The inclusion of nutrients allows to differentiate the proliferative region from the quiescent region of the spheroid, in which the amount of nutrients is not sufficient to maintain cell proliferation (i.e., $c_n \le c_{n0}$). In order to insert the dependency on nutrients in the growth term, it is necessary to give the evolution of these chemicals inside the spheroid. Nutrients diffuse inside the tissue and are transported by the liquid moving in the interstitial space, so that the mass balance for nutrients dissolved in the liquid phase, in Lagrangian coordinates, reads [26]

$$\dot{c}_n = \frac{1}{\nu\phi_\ell}\left(\mathbf{F}^{-1}\mathbf{K}(\phi_s)\mathbf{F}^{-T}\,\mathrm{Grad}\,p\right)\cdot\,\mathrm{Grad}\,c_n + \frac{1}{J\phi_\ell}\mathrm{Div}\left(J\mathbf{F}^{-1}D_n\mathbf{F}^{-T}\,\mathrm{Grad}\,c_n\right) - \zeta\frac{\phi_s}{\phi_\ell}c_n\,, \tag{12}$$

where c_n is the mass concentration of the nutrients, ζ is the rate of consumption of nutrients for cell biological functions and D_n is the diffusion coefficient of nutrients.
The system of equations (3), (4), (5), (6), (10), (11), (12), which hold in the internal points of $\mathscr{B}_r$, completed with proper conditions prescribed on the boundary $\partial\mathscr{B}_r$, completely defines the growth and remodelling of a tumour mass in response to nutrients.

2.2. Spherical symmetry

Assuming that the initial spherical geometry is preserved throughout the process, the model presented in Section 2.1 is used to describe the isotropic growth and remodelling of a tumour spheroid. Therefore it is reasonable to rewrite the system of eqs. (3)-(6), (10)-(12) in material spherical coordinates, (R, Θ, Φ), considering deformations and velocities of all constituents to be along the R-axis and to depend on R and t only. Therefore we have

$$r(t, \boldsymbol{X}) = \chi(t, R), \qquad \vartheta(t, \boldsymbol{X}) = \Theta, \qquad \varphi(t, \boldsymbol{X}) = \Phi, \tag{13}$$

so that the matrix representation of the deformation gradient tensor is diagonal and given by

$$\mathbf{F} = \mathrm{diag}\left\{\frac{\partial\chi}{\partial R}, \frac{\chi}{R}, \frac{\chi}{R}\right\} \tag{14}$$

and therefore $J = \frac{\partial \chi}{\partial R}\frac{\chi^2}{R^2}$. Then, being $J_p = 1$, and enforcing spherical symmetry, we take

$$\mathbf{F}_p = \mathrm{diag}\left\{\frac{R^2}{\Psi_p^2}, \frac{\Psi_p}{R}, \frac{\Psi_p}{R}\right\}, \tag{15}$$

where Ψ_p is a measure of the remodelling of the spheroids, and we consider a spherical growth

$$\mathbf{F}_g = \mathrm{diag}\left\{g, g, g\right\}. \tag{16}$$

Finally, we assume that the medium is isotropic with respect to both its elastic properties and permeability. In particular, the tensor $\mathbf{K} = K(\phi_s)\mathbf{I}$ is taken from [31] and adapted to our framework, i.e.,

$$K(\phi_s) = k_p\left[\frac{\phi_{s0}}{1-\phi_{s0}}\frac{J-\phi_{sn}J_g}{J_g\phi_{sn}}\right]^{m_0}\exp\left\{\frac{m_1}{2}\left[\frac{J^2-J_g^2}{J_g^2}\right]\right\}. \tag{17}$$

Taking a spheroid of initial radius, $R = R_{out}$ with an internal calcified core of radius R_0, the following system of equations, derived from (3)-(6), (10)-(12), holds for $R_0 < R < R_{out}$

$$\dot{J} = \frac{1}{\nu}\frac{\chi^2}{R^2}\frac{\partial}{\partial R}(K(\phi_s)\Pi^R) + 2\frac{K(\phi_s)}{\nu}\frac{J}{\chi}\Pi^R \tag{18}$$

$$\dot{g} = \frac{\gamma_s}{3}(\phi_{max}-\phi_s)(c_n - c_{n0})_+ g \tag{19}$$

$$\dot{\Psi}_p = -\frac{J\phi_s}{6\lambda}\left[\left|\frac{J^2\Psi_p^6-\chi^6}{g^2\Psi_p^2\chi^4}\right| - \frac{2\tau}{\mu\phi_s}\right]_+ \mathrm{sign}\left(J^2\Psi_p^6-\chi^6\right)\Psi_p \tag{20}$$

$$\dot{c}_n = \frac{1}{\nu}\frac{\chi^2}{J\phi_\ell R^2}K(\phi_s)\Pi^R\frac{\partial c_n}{\partial R} + \frac{D_n}{J(1-\phi_s)R^2}\frac{\partial}{\partial R}\left(\frac{\chi^4}{JR^2}\frac{\partial c_n}{\partial R}\right) - \zeta\frac{\phi_s}{\phi_\ell}c_n, \tag{21}$$

In (18) and (21), Π^R is the radial component of the material gradient of pressure pulled-forward to the actual configuration, that in spherical coordinates reads

$$\Pi^R = \frac{1}{J}\left[\frac{\partial}{\partial R}(P_s^*)^{rR} + \frac{2}{R}\left((P_s^*)^{rR} - (P_s^*)^{\vartheta\Theta}\right)\right], \tag{22}$$

where $\mathbf{P}_s^* = \mathrm{diag}\left((P_s^*)^{rR}, (P_s^*)^{\vartheta\Theta}, (P_s^*)^{\varphi\Phi}\right)$ is the constitutive part of the first Piola-Kirchoff stress tensor of the cellular component, given by the constitutive equation (9) and the Piola transformation

$$(P_s^*)^{rR} = -J\phi_s\left(\Sigma(\phi_s) + \frac{1}{3}\mu\frac{J^2\Psi_p^6+2\chi^6}{g^2\Psi_p^2\chi^4}\right)\frac{\chi^2}{JR^2} + J\phi_s\mu\frac{J^2\Psi_p^4}{\chi^2 g^2 R^2} \tag{23}$$

$$(P_s^*)^{\vartheta\Theta} = (P_s^*)^{\varphi\Phi} = -J\phi_s\left(\Sigma(\phi_s) + \frac{1}{3}\mu\frac{J^2\Psi_p^6+2\chi^6}{g^2\Psi_p^2\chi^4}\right)\frac{R}{\chi} + J\phi_s\mu\frac{\chi R}{g^2\Psi_p^2}. \tag{24}$$

In (20), we defined the *intracellular-reorganization time* (or *plastic rearrangement time*) $\lambda = \eta/\mu$ and we used the Tresca criterion in order to give a representation of frame invariant measure of the stress present in (10), i.e., $f(\mathbf{T}_s') = |(T_s^{rr})' - (T_s^{\vartheta\vartheta})'|/2$.
Finally, the evolution of the pressure inside the aggregate can be solved a posteriori, once the other unknowns have been determined, using eq. (6) rewritten in spherical coordinates

$$\frac{\partial}{\partial R}p(t,R) = J\frac{R^2}{\chi^2}\Pi^R. \tag{25}$$

We remark that the system of equations (18)-(21) has to be solved together with the auxiliary condition

$$\frac{\partial}{\partial R}\chi = J\frac{R^2}{\chi^2}, \tag{26}$$

and should be supplied by proper boundary conditions (BCs) and initial conditions (ICs) for the unknowns. As initial conditions, we consider that no elastic, plastic and growth deformations are already present and that nutrients are concentrated close to the external boundary, i.e.,

$$J(0,R) = 1 \tag{27}$$
$$\Psi_p(0,R) = R \tag{28}$$
$$g(0,R) = 1 \tag{29}$$
$$c_n(0,R) = e^{-(R-R_{out})^2/\epsilon^2} \tag{30}$$

Regarding the boundary conditions, the mass balance (18) and the diffusion equation (21) require two BCs, whereas eq. (26) is well defined provided that one BC is given. At the MCTS external boundary, located in R_{out}, boundary conditions have to be consistent with the following requirements:

(i) the radial stress at the external boundary of the specimen has to be equal to the applied stress, $P_{appl}(t)$;

(ii) the pressure p has to vanish at $R = R_{out}$ since the liquid is in equilibrium with the liquid outside the spheroid.

(iii) the nutrient concentration c_n is maintained constant and equal to c_b in the external nutrient-rich environment

These observations are translated in the following set of boundary conditions

$$(T_s^*)^{rr}(t,\chi(R_{out})) = P_{appl}(t) \tag{31}$$
$$p(t,\chi(t,R_{out})) = 0 \tag{32}$$
$$c_n(t,\chi(t,R_{out})) = c_b\,. \tag{33}$$

The boundary condition (31) looks like a Dirichlet condition on J at the external boundary, since, for the particular form of $\Sigma(\phi_s)$ that we chose,

$$\left[-\phi_s\left(E\frac{\phi_s-\phi_0}{\phi_{max}-\phi_s}+\mu\frac{1}{3}\frac{J^2\Psi_p^6+2\chi^6}{g^2\Psi_p^2\chi^4}\right)+\mu\phi_s\frac{J^2\Psi_p^4}{\chi^4 g^2}\right]_{\chi(t,R_{out})} = P_{appl}(t)\,. \tag{34}$$

This equation is nonlinear with respect to $J(t,R_{out})$ and solutions can be found by applying Newton's method or other techniques.
For what concerns the inner boundary located in R_0, we have to distinguish the case in which the necrotic core is either calcified or composed by a liquid cavity. In the first case

(iv-n) the velocities of the fluid and of solid phases have to vanish at the inner boundary because the calcified necrotic core is assumed impervious,

(v-n) since the necrotic process occurs over longer scales than those related to growth and remodelling, we can consider a fixed boundary between the necrotic core and the quiescent region,

(vi-n) the rigid necrotic core is impermeable to nutrients,

so that

$$\chi(t,R_0) = R_0 \tag{35}$$
$$\Pi^R(t,R_0) = 0 \tag{36}$$
$$\frac{\partial c_n}{\partial R}(t,R_0) = 0\,. \tag{37}$$

Indeed (35) guaranties that the interface between the necrotic calcified core and the surrounding living cells is fixed, whereas (36), which is a Robin BC for J at the inner boundary, states that the flux at the inner

boundary is null, being velocities null.
On the other hand, when we consider the case of spheroids with a necrotic liquid core, we cannot assume that the inner boundary of the spheroid is impermeable and fixed. In this case, the BCs in R_0 should be consistent with the following requirements:

(iv-l) the radial stress exerted by the mixture equals the liquid core radial stress, T_ℓ^{rr},

(v-l) the flux at the inner boundary is preserved and the inner boundary moves with the solid phase,

(vi-l) inside the necrotic liquid region, the concentration of nutrients is homogeneously distributed,

that are translated in the following set of boundary conditions

$$\dot{\chi}(t,R_0) = \boldsymbol{v}_s^R \quad \Longrightarrow \quad \dot{\chi}(t,R_0) = \frac{K(\phi_s)}{\nu}\Pi^R \tag{38}$$

$$T_m^{rr}(t,\chi(t,R_0)) = T_\ell^{rr}(t,\chi(t,R_0)) \quad \Longrightarrow \quad (T_s^*)^{rr}(t,\chi(t,R_0)) = 0 \tag{39}$$

$$\frac{\partial c_n}{\partial R}(t,R_0) = 0 \tag{40}$$

The boundary condition (38) can be obtained by the mass-balance equation of the liquid and the cellular phase for an incompressible, closed and saturated mixture, which written in spherical coordinates entails

$$\frac{\partial}{\partial r}\left(r^2(\phi_s\boldsymbol{v}_s + \phi_\ell\boldsymbol{v}_\ell)\right) = 0\,. \tag{41}$$

Being $\boldsymbol{v} = \phi_s\boldsymbol{v}_s + \phi_\ell\boldsymbol{v}_\ell$ continuous across the interface and $\boldsymbol{v} = 0$ in the liquid core, we have

$$\boldsymbol{v}_\ell = -\frac{\phi_s}{\phi_\ell}\boldsymbol{v}_s \tag{42}$$

in the whole MCTS domain, which coupled with the Darcy equation (4) leads to (38). As observed for the outer boundary, eq. (39) can be rephrased in

$$\left[-\phi_s\left(E\frac{\phi_s-\phi_0}{\phi_{max}-\phi_s} + \frac{1}{3}\mu\frac{J^2\Psi_p^6 + 2\chi^6}{g^2\Psi_p^2\chi^4}\right) + \mu\phi_s\frac{J^2\Psi_p^4}{\chi^4 g^2}\right]_{\chi(t,R_0)} = 0 \tag{43}$$

that is a non-linear Dirichlet condition on J.

3. Results

In this section, we first present the results of a quiescent spheroid undergoing pure remodelling due to the application of an external load on the outer boundary (Section 3.1), and, then, we consider the case of a MCTS with an external proliferative ring, an intermediate quiescent region, determined by nutrients availability, and a necrotic core (Section 3.2). In both cases we will analyze either the presence of a fully calcified necrotic core or the presence of a cavity filled with water, inside the aggregate.
The results in this section are presented in terms of dimensionless quantities. Indeed, the parameters in the model may vary significantly considering different types of tumour cells [19, 21, 29, 61, 66], therefore a dimensionless approach is more valuable in analyzing the relative influence of single and interrelated parameters on the overall process. Spatial quantities are scaled with respect to the initial external radius of the spheroid, R_{out}, whereas temporal quantities scale with the typical cell proliferation time, $t_r = (\phi_{max}\gamma_s c_b)^{-1}$; stresses and mechanical parameters are made dimensionless with respect to the shear modulus of the material, μ, the volume fractions are compared to the maximum cellular volume fraction, ϕ_{max}, while the nutrient concentration is related to the concentration at the external boundary, c_b. Thus, the following dimensionless quantities are introduced

$$\tilde{R} = \frac{R}{R_{out}}\,, \quad \tilde{r} = \tilde{\chi} = \frac{\chi}{R_{out}}, \quad \tilde{\Psi}_p = \frac{\Psi_p}{R_{out}}\,, \quad \tilde{t} = \frac{t}{t_r}\,, \quad \tilde{\phi}_s = \frac{\phi_s}{\phi_{max}}\,, \quad \tilde{c}_n = \frac{c_n}{c_b}\,,$$

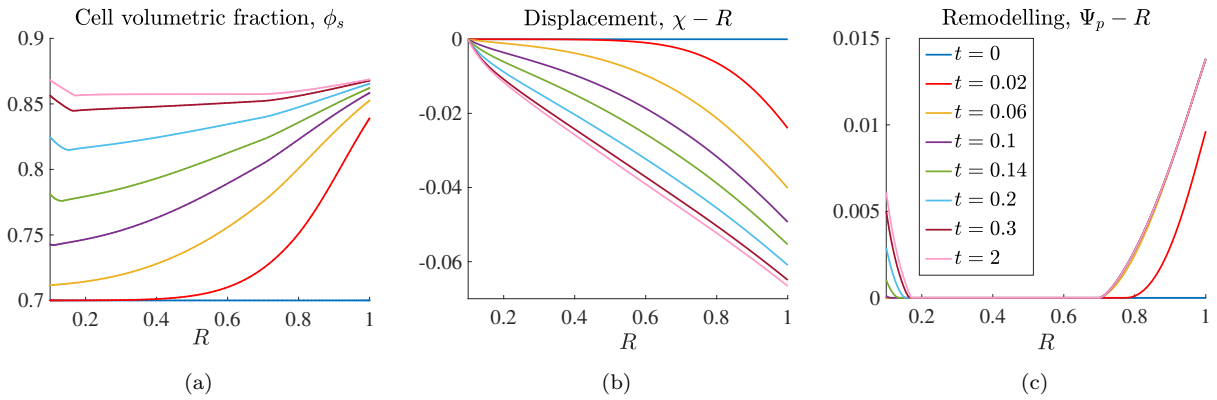

Figure 3: Calcified core without growth: simulations for dimensionless parameters $P_{appl} = -0.28$, $k_p = 0.77$, $m_0 = 0.0848$, $m_1 = 4.638$, $\tau = 0.028$, $\lambda = 0.028$, $E = 0.28$. Lines report the evolution in space of (a) the cell volumetric fraction ϕ_s, (b) the MSCT displacement, $\chi - R$ and (c) the plastic remodelling $\Psi_p - R$ at the instant of time specified in the legend. For the final time reported in the figures, the system is at the stationary condition.

$$\tilde{P}_{appl} = \frac{P_{appl}}{\mu\phi_{max}}\,, \quad (\tilde{P}_s^*)^{rR} = \frac{(P_s^*)^{rR}}{\mu\phi_{max}}\,, \quad (\tilde{P}_s^*)^{\vartheta\Theta} = \frac{(P_s^*)^{\vartheta\Theta}}{\mu\phi_{max}}\,, \quad \tilde{\tau}(\tilde{\phi}_s) = \frac{\tau(\phi_s)}{\mu\phi_{max}}\,, \quad \tilde{E} = \frac{E}{\mu}\,,$$
$$\tilde{k}_p = \frac{k_0\mu\phi_{max}t_r}{\nu R_{out}^2}\,, \quad \tilde{D}_n = \frac{D_n t_r}{\phi_{max}R_{out}^2}\,, \quad \tilde{\zeta} = \zeta t_r\,, \quad \tilde{\lambda} = \frac{\lambda}{t_r}\,, \quad \tilde{c}_0 = \frac{c_0}{c_b}\,.$$

In the following, for sake of simplicity in the notation, we will drop the $\tilde{(\cdot)}$ and all the quantities reported are dimensionless.

The numerical results have been obtained by discretizing the one dimensional dimensionless domain, represented by the interval $[R_0, 1]$, into $N + 1$ subintervals of varying width, through the introduction of N Chebyshev nodes in $(R_0, 1)$, so that the discretization is denser closer to the inner and outer boundaries. According to this procedure, the initial system of partial differential equations (18)-(21) is approximated by a system of ordinary differential equations that can be integrated by an explicit Euler scheme in time. The variation of pressure inside the specimen can be calculated a posteriori, once Π^R is known, using (25), that can be solved with a forward Euler scheme in space.

3.1. Tumour response to an external stress, without growth

In this section, we simulate the mechanical behaviour of a spheroid with a necrotic core of radius R_0 (that can be either composed of calcified debris, i.e., rigid, or filled with liquid) and an external quiescent shell (in which cell proliferation is compensated by death), subjected to a known load applied on the outer boundary. The external load represents the controlled stress exerted in vitro by the gel in which cancer cells are cultured and it mimics the stress applied by the external tissue in vivo. In this case, we do not consider growth, since the time of application of the load can be shorter compared to the typical time required by growth [41]. Therefore in this case we do not have any net production of the cellular phase, i.e., $\Gamma_s = 0$ in (19), which implies $g(t, R) = 1\,, \forall t$ and $\forall R$. The evolution of the system is, then, obtained by solving eqs. (18), (20), (26), coupled with the initial conditions (27) and (28), the boundary condition at the external boundary (34) and either the BCS (35)-(36) when the rigid necrotic core is studied or (38)-(39) for the liquid core.

In particular, we focus on different behaviours of the MCTS depending on its capability to reorganize in response to the external load, presenting both the case in which remodelling occurs (setting a small value of the parameter τ, so that the stress is above the set threshold in a portion of the aggregate) in Figs. 3 and 5, and the case in which no plastic reorganization occurs (higher value of the parameter τ) in Fig. 6. We remark that if no stress is applied at the outer boundary, the stationary case corresponds to the initial condition, i.e. we do not have any evolution of the system.

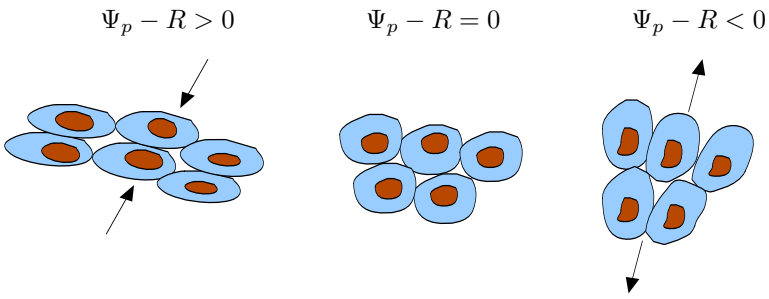

Figure 4: Diagram of the possible internal reorganization occurring inside a spheroid: remodelling through compression (on the left), physiological condition (centre), remodelling through extension (on the right).

Fig. 3 shows the evolution in time and space of $\phi_s(t,R) = \phi_{sn}/J(t,R)$, $\Psi_p(t,R) - R$ and $\chi(t,R) - R$ for a spheroid with a calcified core subjected to a constant stress at the outer boundary able to trigger the internal remodelling of the aggregate. Every curve represents the trend over R of the different quantities at a fixed time step (see legend). It is possible to see that, in the first time steps, the cell volumetric fraction strongly increases at the outer boundary where the load is applied. Then the whole aggregate is strongly compressed (see Fig. 3-(a)) and its volume diminishes (i.e. J decreases, being J inversely proportional to ϕ_s), as it is clear from the negative displacement in Fig. 3-(b). In the case of a calcified necrotic core, due to the BC (35) the displacement is null in proximity of the necrotic core, whereas the spheroid radius decreases until the stationary condition is reached. We remark that after $t \approx 0.1$ the trend in the curves representing the distribution of ϕ_s changes in proximity of the internal boundary. This change corresponds to the activation of the internal reorganization close to the inner boundary (see Fig. 3-(c)). Indeed, while the remodelling at the external boundary starts as soon as the load is applied and after $t \approx 0.06$ the region close to R_{out} has completely reorganized, the layer close to the necrotic core starts deforming plastically only at a later time (i.e., $t > 0.1$). For better understanding the meaning of the remodelling term, we remark that $F_p^{rR} = R^2/\Psi_p^2$, whereas $F_p^{\theta\Theta} = F_p^{\phi\Phi} = \Psi_p/R$, thus

- $\Psi_p - R < 0 \iff F_p^{rR} > 1$ and $F_p^{\theta\Theta} = F_p^{\phi\Phi} < 1$, which means that remodelling occurs through extensions along the radial direction and compression in the transverse directions;
- $\Psi_p - R > 0 \iff F_p^{rR} < 1$ and $F_p^{\theta\Theta} = F_p^{\phi\Phi} > 1$, which means that remodelling occurs through compression along the R-axis and extensions along the Θ and Φ directions.

Fig. 4 intuitively explains the biological meaning of the remodelling term.

Therefore, when a calcified quiescent MCTS is compressed, as shown in Fig. 3-(c), in the first instants of time, consistent remodelling occurs at the external boundary due to compression along the radial direction and extension along the angular directions, as a consequence of the external compression load. Then remodelling at the external boundary reaches the steady state condition (indeed, for the specific parameters used in Fig. 3, after $t \approx 0.06$ the curves at the external boundary almost overlap), while remodelling starts at the internal boundary where cells are constrained not to penetrate the necrotic core. Close to the internal boundary, $\Psi_p - R > 0$, being cell compressed towards the necrotic core. Also in this case, remodelling continues until a stationary condition is reached (after $t \approx 2$). We remark that, thanks to the remodelling occurring in the region near the calcified core and in the outer region, ϕ_s is higher than in the central region, where remodelling is not triggered. Therefore the effect of bond rupture, when the aggregate is constrained on both sides, leads to a closer packaging of cells.

Moreover we observe that, for the parameters set in this simulations, remodelling occurs only in some regions of the aggregate. Therefore we have that the mechanical behaviour of the aggregate changes in space: in the central region it behaves visco-elastically, whereas close to the inner and the outer boundary it behaves as an visco-elasto-plastic material. This difference in the mechanical response of cells leads to a highly non-homogeneous distribution of cells inside the domain.

Looking at the liquid core case, in Fig. 5, we observe that, also in this case, in the first instants of time, cells are more compressed at the outer boundary (Fig. 5-(a)), then, as the deformation of the aggregate

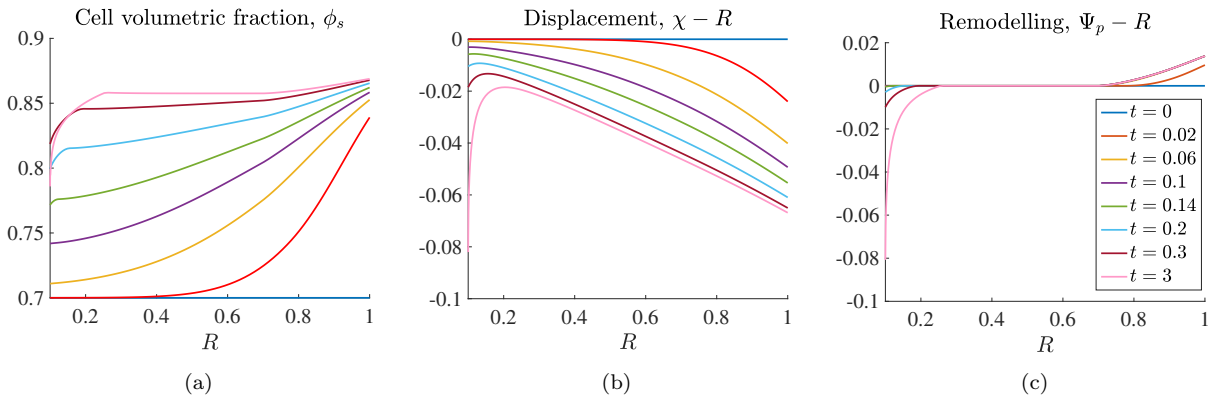

Figure 5: Liquid core without growth: simulations for the same values of the parameters used in the simulation of the calcified core. Lines report the evolution in space of the variables at the instant of time specified. We remark that in this case at time $t = 3$ the steady state is not yet reached. Indeed, for the liquid core undergoing remodelling the internal boundary continues to move until cells fill all the internal gap.

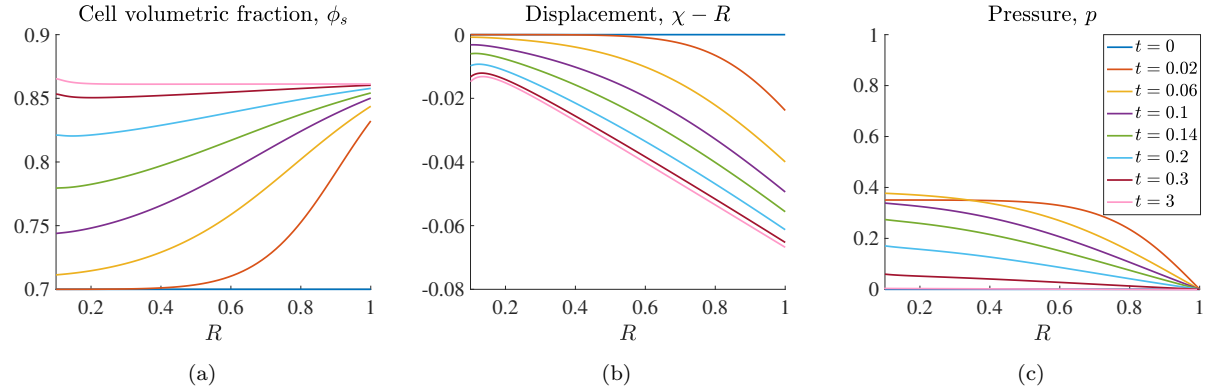

Figure 6: Liquid core without growth and without remodelling: simulations for the same values of the parameters used in the simulation of the calcified core, but for a value of τ for which no remodelling occurs. Lines report the evolution in space of the variable at the instant of time specified. We remark that at the stationary state (after $t \approx 3$) there is still some liquid in the central necrotic core.

increases (see Fig. 5-(b)), cells volumetric fraction increases in the whole domain. However, in this case, the solid volumetric fraction in the region near the necrotic core is less influenced by the application of an external load, being cells not pushed against a rigid wall. Indeed in this case, cells can move toward the liquid core, as fluid encapsulated inside the central core flows through the aggregate, leading to the decrease of the central liquid core radius ($\chi(t, R_0) - R_0 < 0$ in Fig. 5-(b)). In this case, for $t = 3$ the steady state condition, which corresponds to the compressed cells filling the whole necrotic cavity, is not reached yet.
Moreover, consistent remodelling initially occurs at the external boundary, due to compression along the R direction and extension along the transverse directions, as seen for the calcified necrotic core, due to the application of the external load. At variance with what happens in presence of a necrotic core, in this case, at the internal boundary, $\Psi_p - R$ is negative which means that remodelling occurs through extension along the R-axis. Indeed, when a liquid cavity forms the center of the MCTS, the effect of bond rupture is to allow cells to move freely towards the central necrotic core, as long as it is all filled by cells. Also in this case remodelling is triggered only in some regions of the aggregate, leading to different mechanical behaviours in different MCTS layers.
Conversely, Fig. 6 reports the value of $\phi_s(t, R)$, $\chi(t, R) - R$ and $p(t, R)$ in the case in which a quiescent

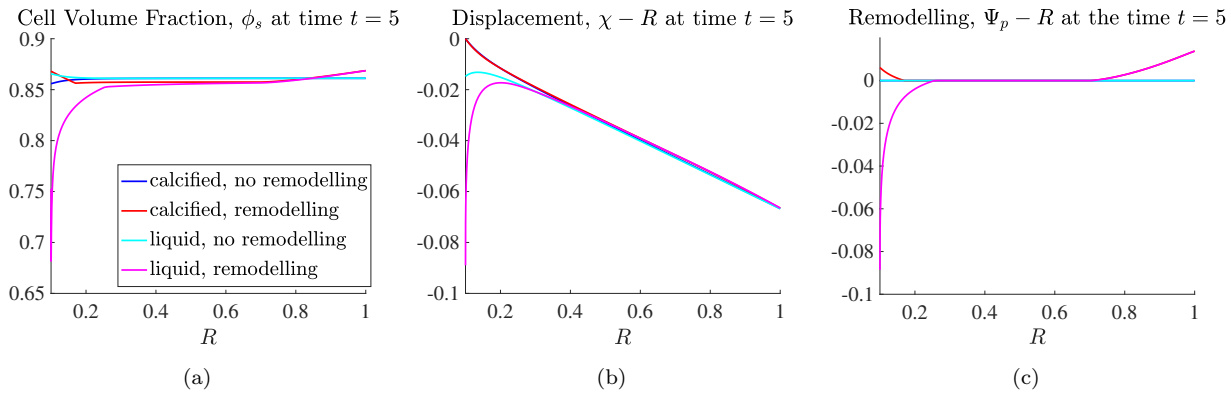

Figure 7: Effect of remodelling on a quiescent aggregate subjected to an external load: comparison between liquid core and calcified core. All variables are reported at time $t = 5$, for which the spheroid with a calcified necrotic core and the one with a liquid core not undergoing remodelling are at the stationary condition.

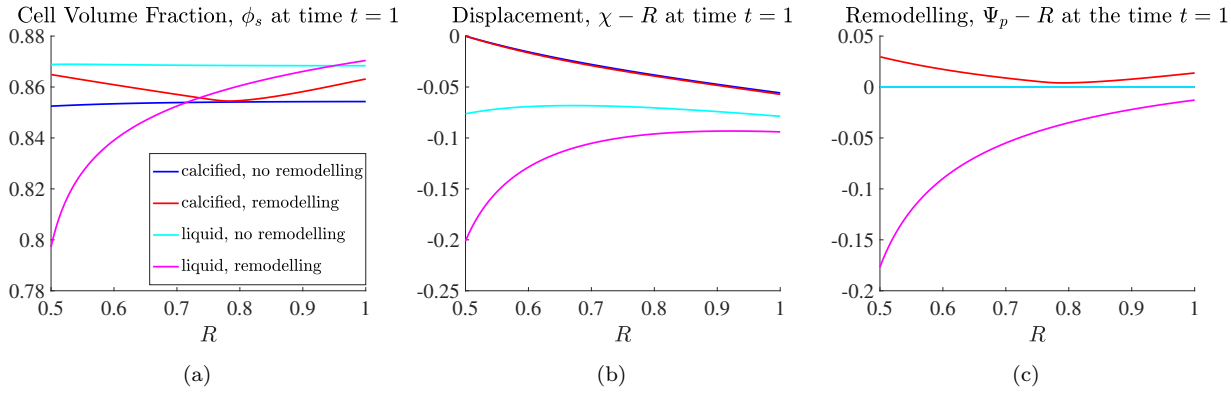

Figure 8: Effect of remodelling on a quiescent aggregate subjected to an external load: comparison between liquid core and calcified core for a MCTS with a necrotic core of radius $R_0 = 0.5$ (all variables are reported at time, $t = 1$).

aggregate with a liquid necrotic core is compressed, without experiencing remodelling. The distribution of ϕ_s inside the MCTS, in this case, is almost constant, with only a slightly increase in the region close to the inner liquid core, which is compressed. Differently from what observed in the elasto-plastic case, at the steady state (which is reached at $t \approx 3$), when p is null everywhere inside the spheroid (Fig. 6-(c)), so that $\mathbf{v}_c = 0$, the internal liquid core is not fully filled by cells (see Fig. 6-(b)).

For a clearer comparison among the different cases, Fig. 7 reports the values of $\phi_s(t, R)$, $\chi(t, R) - R$ and $\Psi_p(t, R) - R$ at the reference time $t = 5$, both for the calcified core with and without remodelling (red and blue curves, respectively) and the liquid core with and without remodelling (purple and light-blue curves, respectively). Fig. 7 shows that, both for the calcified core and the liquid one, where remodelling is triggered, cells are more closely packed than in the region in which remodelling does not occurs. Thus, at the internal and external boundaries, the cell volumetric fraction is higher than in the central region. However, while at the external border the behaviour of the MCTS with either a calcified or a liquid core is the same, at the internal boundary, remodelling in the liquid core strives to maintain the cell volumetric fraction closer to the physiological value and thus, when it is triggered, less intense volumetric changes are perceived in proximity of the necrotic region. Indeed, in this case, the rupture of bonds leads to more intense cell movements toward the central necrotic region and thus more intense displacement are recorded at the interface between the necrotic and the quiescent regions. When no remodelling is triggered, the displacement of the cell phase at

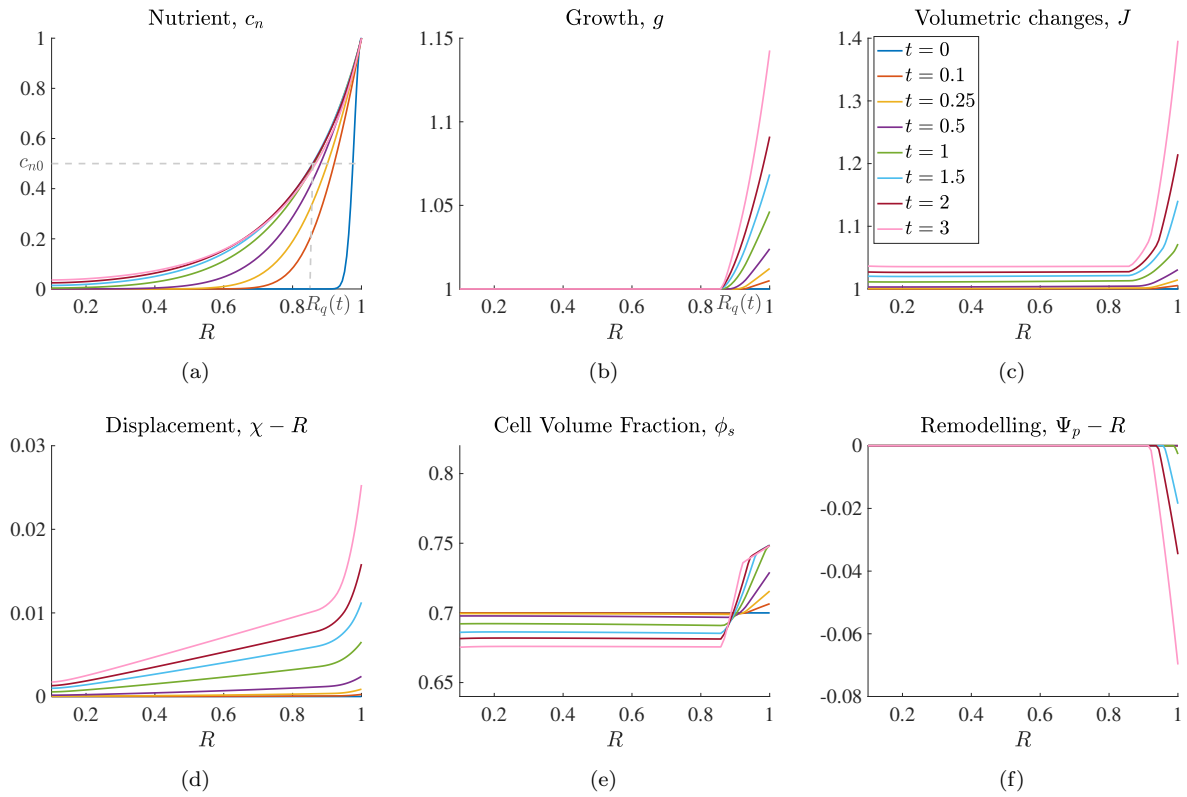

Figure 9: Free growth of a spheroid with a liquid core, a quiescent region and an external proliferative ring. The parameters are the same as in the simulation in fig. 3, except for $k_p = 0.7745$, $c_{n0} = 0.5$, $D_n = 0.01$ and $\zeta = 0.5$.

the interior boundary is smaller and so ϕ_s should increase, to preserve the total spheroid mass. Finally, in the case in which remodelling does not occur, being the mechanical behaviour of the aggregate the same in the whole domain, the curves are smoother, both in the presence of the calcified and of the liquid core.

The influence of the composition (i.e., calcified vs. liquid) of the inner region on the mechanical behaviour of the whole aggregate is more evident when the size of the necrotic core is larger. In particular, in Fig. 8 we report the case in which the tumour spheroid is 12.5% necrotic by volume (i.e. $R_0 = 0.5$). In this case, not only the occurrence of remodelling, but also the mechanical properties of the central region play a fundamental role in determining the distribution of the cell volume fraction (Fig. 8-(a)) and displacements inside the spheroid (Fig. 8-(b)). In particular, the MCTSs with the liquid cavity can be easily compressed by the external load, so that the displacement at the outer boundary is higher in case in which the spheroid has a liquid necrotic core, with respect to the calcified aggregate (Fig. 8-(b)). When remodelling is triggered, in the case of a liquid necrotic core, high displacements are recorded both at the inner and at the outer boundary, so that while the radius of the compressed spheroid decreases ($\chi(t,1) < 1$), the extension of the quiescent region increases (in Fig. 8-(b), $\chi(t,R_0) - R_0 < \chi(t,1) - 1 \implies \chi(t,1) - \chi(t,R_0) > 1 - R_0$ for the magenta curve) and the remodelling in the MCTS occurs through extension along the radial direction ($\Psi_p - R < 0$ in Fig. 8-(c), magenta curve). Conversely, when the aggregate is compressed against the rigid calcified core, the remodelling is due to compression along the radial direction ($\Psi_p - R > 0$ in Fig. 8-(c), red curve).

3.2. Growth and remodelling of a tumour spheroid

In this section we include the growth of the spheroid guided by nutrients availability also considering the application of a load on the outer boundary, that compresses the spheroid. Therefore the evolution of

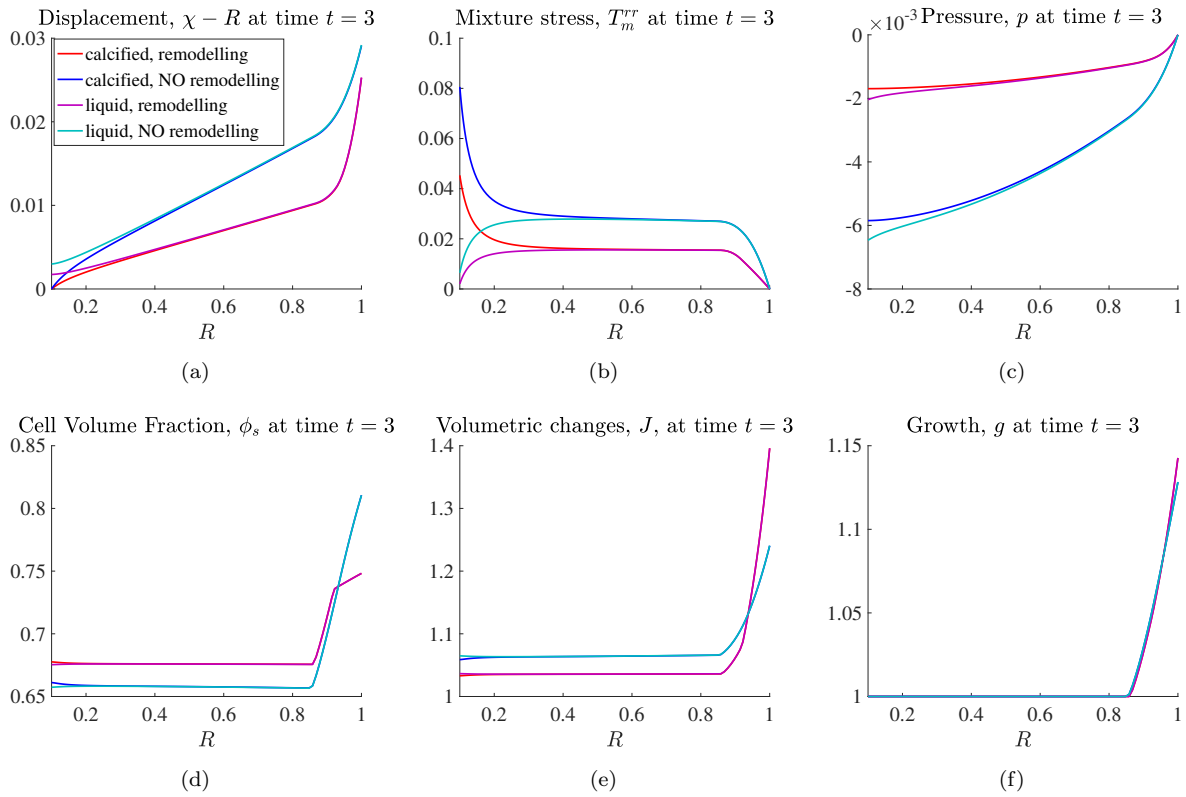

Figure 10: Effect of remodelling and free growth on a proliferative MCTS with a quiescent layer and a necrotic core, either liquid or calcified (all variables are reported at time $t = 3$).

the system is obtained by solving eqs. (18)-(21) and (26), coupled with the initial conditions (27)-(30), the boundary conditions at the external boundary (33),(34) and either the BCS (35),(36),(37) when the rigid necrotic core is studied or (38),(39),(40) for the liquid core. In particular, we first look at the free growth of a MCTS, i.e., when no load is applied at the outer boundary ($P_{appl} = 0$ in the simulations), in order to let the aggregate freely expand and study the remodelling triggered by the pure growth inside the structure. The variation in time and space of the different variables of the model, when there is a liquid cavity inside the aggregate and remodelling occurs, are shown in Fig. 9.

Nutrients diffuse and are transported by the fluid moving inside the spheroid, from the outer environment, and their concentration is high enough to guarantee the proliferation of cells, only in the region close to the external boundary, (see Fig. 9-(a)). The radius of the quiescent region $R_q(t)$, in which the nutrients are below the set threshold for proliferation, $c_n < c_{n0}$, depends on time and is regulated by the nutrient diffusive length and by the expansion of the aggregate. Therefore $g(t, R) > 1$ only in the external portion of the tumour spheroid, i.e., $R > R_q(t)$, which corresponds to the proliferative shell (see Fig. 9-(b)), whereas for $R_0 < R \leq R_q(t)$, we have $g(t, R) = 1$ (quiescent region). The sharp transition between the proliferative ring and the quiescent region is qualitatively in agreement with biological experiments [12, 18, 28], highlighting the existence of a well-definded external rim in which cells duplicate and only some isolated cells proliferating inside the quiescent region [28]. Even though also other factors (e.g. external environment, stresses, ...) can play a crucial role in the growth of MCTSs, the thickness of the proliferative rim correlates with the diffusive limit of oxygen and eventually other nutrients [12, 18, 28], estimated from images of the sections of dual-stained MCTS with specific markers for proliferation and hypoxia.
Numerical simulations also show that the highest volumetric changes occur at the boundary of the tumour, where the aggregate grows. In the case of the MCTS free growth, $J(t, R) > 1$ in the whole aggregate, which

denotes the expansion of the tumour mass (Fig. 9-(c)). The enlargement of the aggregate is evident also from the displacement plot (see Fig. 9-(d)). In the case of an inner liquid core, even though in the very first instants of time the inner boundary slightly penetrates the cavity (not shown in the figure), then the expansion of the whole structure makes the necrotic core and the quiescent region, expand, too, dragged by the proliferative rim. Since the quiescent region enlargement is not compensated by cell growth the cell volumetric fraction decreases there (see Fig. 9-(e)), whereas in the proliferative outer layer the tumour cell volumetric fraction rapidly increases, leading to lines crossing over each other in the cell volumetric plot. The void spaces in the expanding quiescent and necrotic regions are filled by the liquid moving towards the center of the MCTS. The higher amount of liquid in the quiescent region with respect to the proliferative region is also confirmed by biological experiments [56], showing a closer-packaging of cells in the external rim and a higher amount of cytoplasmatic liquid, released by cell death, in the quiescent layer.
In the case in which remodelling occurs, closer to the outer boundary, due to the reorganization of the structure (Fig. 9-(f)), the increase of the cellular volume fraction is less pronounced. We remark that in this case, the plastic reorganization of the MCTS is merely due to the stress resulting from the proliferation of cells and not to the application of an external load. Furthermore, for the particular value of remodelling threshold set in the simulations, a portion of the proliferative rim does not experience the plastic reorganization of cells. Therefore, it is possible to virtually divide the proliferative domain into two subregions: the outer portion of the rim undergoes both proliferation and remodelling, whereas the inner part, where the stress due to cell proliferation is not enough to overcome the yield stress, experiences anelastic deformations due to pure growth. The result of this biphasic anelastic behaviour is evident in the cell volumetric distribution, which shows different trends in the two proliferative subregions (Fig. 9-(e)). Of course this effect is dependent on the chosen value of the remodelling threshold. Specifically, for lower values of τ, remodelling can occur in the whole proliferative rim, leading to a smoother distribution of cell volume fraction inside the aggregate. We remark that in the first instants of time, cell proliferation occurs without remodelling (up to $t \approx 0.9$), then remodelling due to extension along the R-direction (i.e., $\Psi_p - R < 0$) only starts in that portion of the proliferative region where cell growth generates sufficient stress inside the structure in order to overcome the chosen yield stress (Fig. 9-(f)).
The effect of remodelling on the distribution of cell growth, stresses, displacements and volumetric changes inside the structure, depending on the mechanical characteristic of the central necrotic core, is transparent in Fig. 10. As observed for the quiescent aggregate, remodelling highly influences the behaviour of a growing MCTS, indeed the biggest differences in the curve in Fig. 10, apart from the region close to the necrotic core, are not related to the mechanical properties of the central tumour region, but to the extent of the plastic reorganizing phenomena occurring among the cells inside the structure. In this case, the differences between the calcified and the liquid necrotic core is even less pronounced than in the case of a non-duplicating MCTS, with appreciable alterations only in the distribution of displacements (Fig.10-(a)), of the mixture stresses (Fig. 10-(b)) and of the fluid interstitial pressure (Fig.10-(c)) in the quiescent region in proximity to the central necrotic region. On the other hand, the mechanical characteristic of the inner core, does not significantly influence the distribution of ϕ_s, J and g (Fig. 10-(d)-(e)-(f), respectively). In the proliferative region the presence of either calcifications or a liquid cavity inside the structure is shaded by the occurrence of plastic phenomena, which strongly alter the behaviour of the system: when no remodelling is triggered, the MCTS experiences lower displacements (Fig. 10-(a)), which are compensated by a higher ϕ_s (and consequently less liquid) in the quiescent region with respect to the case in which remodelling does not occur (Fig. 10-(e)), whereas the effect of remodelling is to reduce cell compaction in the region close to the external boundary, where the MCTS yields.
Finally, we studied the behaviour of a MCTS growing under different imposed loads (specifically, $P_{appl} = -0.1$, in Figs. 11 and 13, and $P_{appl} = -0.28$, in Figs. 12 and 14), that mimic the presence of an external tissue or gel, compressing the tumour mass. In the first instants of time the aggregate is compressed due to the external load, then cells duplication (Figs. 11-(a) and 12-(a)) becomes high enough in order to make the spheroid expand again (see Fig. 11-(b) for $t > 0.5$ and Fig. 12-(b) for $t \geq 1$). While at the beginning of the process (Fig. 11-(c) for $t < 0.5$ and Fig. 12-(c) for $t < 1$) the increase in the volumetric fraction is purely due to the compression of the aggregate, and thus it is distributed inside the whole MCTS, when growth becomes

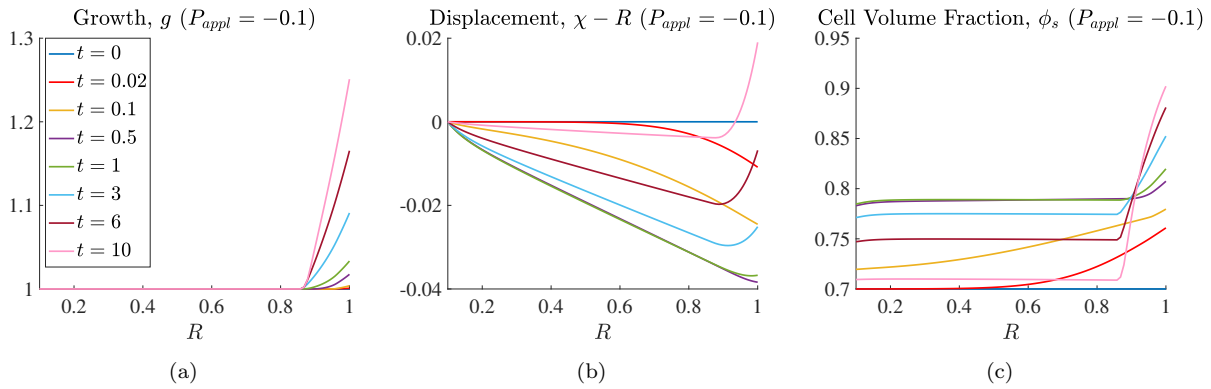

Figure 11: Growth of a spheroid with a calcified core when an external load is applied at the outer boundary. The parameters are the same as in the simulation in Fig. 9, except for $P_{appl} = -0.1$ and τ, which is too high to induce remodelling.

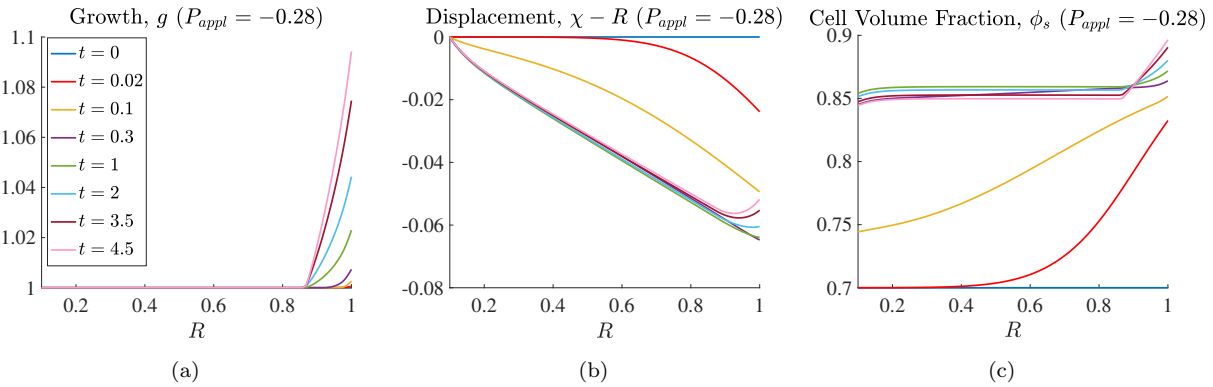

Figure 12: Growth of a spheroid with a calcified core when an external load is applied at the outer boundary. The parameters are the same as in the simulation in Fig. 9, except for $P_{appl} = -0.28$ and τ which is too high to induce remodelling.

consistent, ϕ_s increases accordingly only in the proliferative region. When cell duplication in the external rim prevails over MCTS compression, cell compaction in the quiescent region reduces, due to the expansion of the whole multicellular structure, and cell volumetric fraction approaches the initial physiological value, leading to line crossing in the plots (see Fig. 12-(c)).

As expected, when the applied load is higher (Fig. 12-(b) vs. Fig. 11-(b)), the multicellular spheroid experiences a more intense compression and the growth of the tumour is slowed down. We remark that in both cases, the growth and applied stresses are not sufficient to overcome the threshold set for remodelling, therefore the MCTS does not yield.

On the other hand, as observed in the free-growth cases, when plastic cell reorganization occurs (Fig. 13 and Fig. 14), the curves show abrupt changes in correspondence of the region where anelastic deformations, i.e., remodelling and/or growth, are triggered (i.e., close to the internal and outer boundaries). In particular, looking at the remodelling curves, it is possible to notice that, in the first instants of time, when proliferation is not significant, $\Psi_p - R$ is positive both close to the necrotic core and to the external boundary (Fig. 13-(a) and Fig. 14-(a)), since, in both regions, internal reorganization occurs through compression along the radial direction, as observed for the quiescent aggregate undergoing compression. Then, as proliferation increases, while remodelling at the inner boundary continues to be driven by compression of cells against the rigid calcified wall, at the outer boundary, $\Psi_p - R$ becomes negative, which means that remodelling occurs through a radial extension due to growth (see Fig. 13-(b) and Fig. 14-(b) in proximity of the external

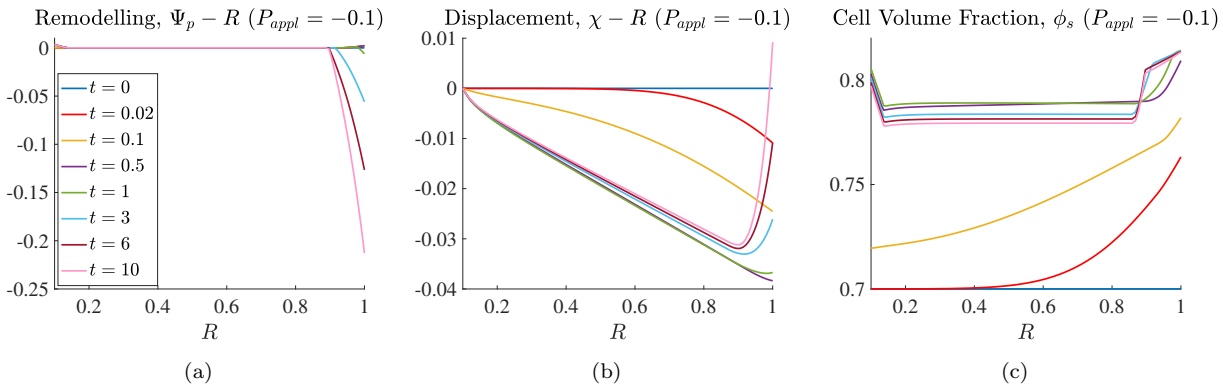

Figure 13: Growth of a spheroid with a calcified core when an external load is applied at the outer boundary. The parameters are the same as in the simulation in Fig. 11, except for the remodelling threshold, $\tau = 0.028$.

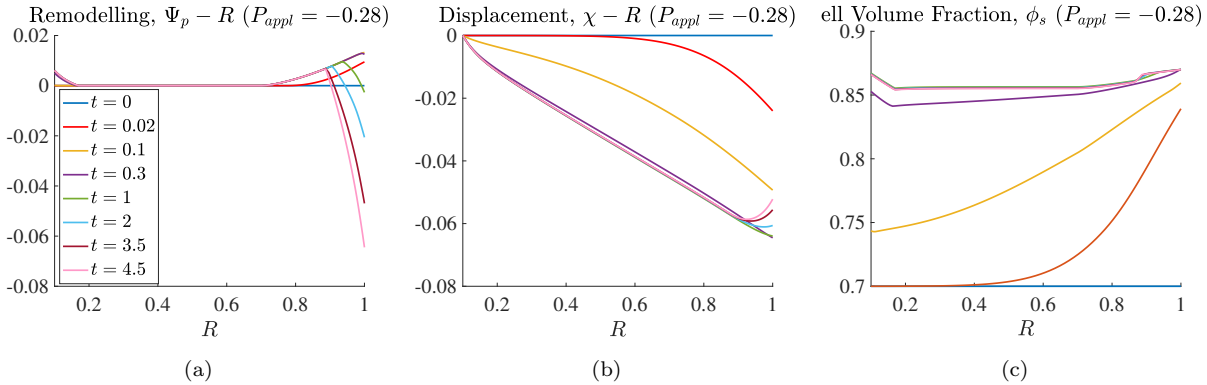

Figure 14: Growth of a spheroid with a calcified core when an external load is applied at the outer boundary. The parameters are the same as in the simulation in Fig. 12, except for the remodelling threshold, $\tau = 0.028$.

boundary). Specifically, in the final instants of the simulations reported in Fig. 13, for the chosen values of yield stress and applied load, remodelling does not involve the whole proliferative region and thus it is possible to virtually distinguish four MCTS subregions (from the core to the outer boundary): the quiescent visco-elasto-plastic layer, the quiescent visco-elastic layer, the proliferative visco-elastic layer and the proliferative visco-elasto-plastic rim. On the other hand, when the external load is higher (see Fig. 14), remodelling occurs in the whole proliferative rim and the distribution of ϕ_s is smoother than in the previous case, even though transitions between the elastic and yielded regions are still clearly visible. In any case, we remark that when remodelling is triggered, the increase in ϕ_s in the proliferative region is slowed down (Fig. 13-(c) and Fig. 14-(c)) with respect to the MCTS that does not experience yield (Fig. 11-(c) and Fig. 12-(c)).
Finally, thanks to the rupture of the bonds among cells, the deformation inside the yielded MCTS rapidly changes going from the proliferative layer to the quiescent one (see Fig. 11-(b) vs. Fig. 13-(b)).

4. Conclusion

In this work we formulated a mathematical model able to reproduce the growth of a tumour spheroid, described as a biphasic material, composed by cells and extracellular liquid. The model is able to take into account anelastic deformations resulting both from growth processes in response to nutrient availability and the internal reorganization of cells, occurring when the stress inside the MCTS is above a given threshold.

The introduction of the liquid phase is essential to properly describe the transport of nutrients, along with their diffusion, from the external boundary of the multicellular aggregate, where they are supposed to be abundant. Furthermore, the introduction of the liquid phase also allows to take into account the existence of a water cavity inside the multicellular structure, due to cell necrosis. The effect of the surrounding environment is included in the present model in term of a given force acting at the external boundary of the spheroid.

In particular, the numerical simulations showed that when an external load is imposed on a quiescent aggregate with a liquid necrotic core, if no remodelling occurs, the aggregate is able to bear the load preserving the inner necrotic cavity. On the other hand when the stress inside the structure is able to drive the intracellular reorganization, bonds break and the aggregate is compacted until the internal liquid core is totally filled by cells. In the case of a MCTS with a solid calcified necrotic core, remodelling leads to a denser spheroid close to the inner and outer boundary, with respect to the case in which plastic reorganization is not triggered. Furthermore, in the case of a quiescent aggregate deforming under an external load, the mechanical properties of the inner core plays a fundamental role in the MCTS mechanical behaviour if the size of the necrotic region is sufficiently high. Indeed, it is found that, in the presence of a tumour spheroid which is 12.5% necrotic by volume, the mechanical response of the cell aggregates to stress can be greatly altered by the presence of the necrotic structure, along with the capability of cells to plastically reorganize. On the other hand, for what concerns the case of a free growing aggregate in response to nutrients diffusing inside it, the influence of the composition of the necrotic core (calcified vs. liquid) is not so remarkable, since in this case the extent of the necrotic region, at least in the first instants of tumour progression is not so wide. Indeed, even though some cells from the quiescent region penetrate the liquid cavity in the first instant of time and then are pulled away by the proliferative cells, allowing the expansion of the liquid core, the total growth of the MCTS is almost the same, independently from the composition of the necrotic region. In the MCTS free growing condition, the total displacement of the structure is influenced by the extent of remodelling: when the growth of cells is high enough to produce the plastic rearrangement of cells, the expansion of the whole structure is lower than in the case in which the aggregate expands without intracellular remodelling. Finally, when considering the growth of a tumour spheroid under an external load imposed on the outer boundary, in the first instant of time the tumour spheroid experiences compression and then cell growth predominates, leading to tumour expansion.

From the modelling point of view, future works need incorporating the evolution of the either liquid or calcified necrotic core due to cell death, by looking at the problem on longer time scales, than the one considered in the present paper. Indeed, remodelling, growth, apoptosis, necrosis and calcification occurs on various time scales, from the cell swelling and lysis occurring in some hours up to calcifications taking on the order of many days to establish [41]. Thus a comprehensive model should link all these temporal scales, possibly supported by experimental measures for different types of carcinoma. Furthermore, while the necrotic process takes place, secretions of some chemicals by necrotic cells may promote inflammation in the neighboring tissue [41], playing a fundamental role in tumour progression. To this aim, the introduction of the surrounding tissue is very important in order to simulate a situation closer to the pathological in-vivo one, and to take into account tumour-stroma interactions. Finally, it is well known that the original spherical symmetry is not preserved over long time scales [60, 61, 20] and solid tumours might develop asymmetric and complex shapes, due eiher to the occurrence of physical instabilities and morphological transitions at their boundary [25, 7, 8, 11, 9, 22] or to inhomogeneities and anisotropies characterizing the external environment. Since irregular contours usually indicate aggressive and infiltrating tumours, some measure of the irregularity of a tumour boundary may serve as a prognostic index for tumour progression [14, 38]. Thus future work should consider the occurrence of physical instabilities at the MCTS boundary and its development in anistropic environment, both performing a stability analysis of a simplified setting and numerically simulating the whole three-dimensional process.

References

References

[1] D. Ambrosi and F. Mollica. *On the mechanics of a growing tumour.* Int. J. Engng. Sci. 40: 1297–1316 (2002).

[2] D. Ambrosi and F. Mollica. *The role of stress in the growth of a multicellular spheroid.* J. Math. Biol. 48: 477–499 (2004).

[3] D. Ambrosi and L. Preziosi. *Cell adhesion mechanisms and stress relaxation in the mechanics of tumours.* Biomech. Model. Mechanobiol. 8: 397–413 (2009).

[4] R.P. Araujo and D.L.S. McElwain. *A history of the study of solid tumour growth: the contribution of mathematical modelling.* Bull. Math. Biol. 66: 1039–1091 (2004).

[5] N. Bellomo, N.K. Li and P.K. Maini. *On the foundations of cancer modelling: Selected topics, speculations and perspectives.* Math. Models Methods Appl. Sci. 18: 593–646 (2008).

[6] C. Breward, H. Byrne and C. Lewis. *The role of cell-cell interactions in a two-phase model for avascular tumor growth.* J. Math. Biol. 45: 125–152 (2002).

[7] H.M. Byrne and M.A.J. Chaplain. *Growth of non-necrotic tumours in the presence and absence of inhibitors.* Math. Biosci. 130: 151–181 (1995).

[8] H.M. Byrne and M.A.J. Chaplain. *Growth of necrotic tumours in the presence and absence of inhibitors.* Math. Biosci. 135, 187–216 (1996).

[9] H.M. Byrne and M.A.J. Chaplain. *Free boundary value problems associated with the growth and development of multicellular spheroids.* Eur. J. Appl. Math. 8(6), 639–658 (1997).

[10] H.M. Byrne and M.A.J. Chaplain. *Necrosis and apoptosis: distinct cell loss mechanisms in a mathematical model of avascular tumour growth.* J. Theor. Med. 1(3): 223–235 (1998).

[11] H.M. Byrne and P. Matthews. *Asymmetric growth of models of avascular solid tumours: exploiting symmetries.* IMA J Math. Appl. Med. Biol. 19(1): 1–29 (2002).

[12] S. Chandrasekaran and M.R. King. *Gather round: in vitro tumor spheroids as improved models of in vivo tumors.* J. Bioengineer & Biomedical Sci. 2: e109 (2012).

[13] M.A.J. Chaplain. *Avascular growth, angiogenesis and vascular growth in solid tumors: the mathematical modelling of the stages of tumour development.* Math. Comput. Modelling 23(6): 47–87 (1996).

[14] S.S. Cross and D.W.K. Cotton. *The fractal dimension may be a useful morphometric discriminant in histopathology.* J. Pathol. 166: 409–411 (1992).

[15] J.M. Cheng and S.H. Tirumani, K.W. Kim, S.S. Saboo, J.C. Baez and A.B. Shinagare. *Malignant abdominal rocks: where do they come from?* Canc .Imag. 13(4): 527–539 (2013).

[16] A. Agosti, C. Cattaneo, C. Giverso, D. Ambrosi and P. Ciarletta. *A computational framework for the personalized clinical treatment of glioblastoma multiforme.* Z. Angew. Math. Mech.: 1–21 [in press] (2018).

[17] V. Cristini, X. Li, J.S. Lowengrub and S.M. Wise. *Nonlinear simulation of solid tumor growth using a mixture model: invasion and branching.* J. Math. Biol. 58: 723–763 (2009).

[18] X. Cui, Y. Hartanto and H. Zhang. *Advances in multicellular spheroids formation.* J. R. Soc. Interface 14 (127): 20160877 (2017).

[19] R.E. Durand. *Multicellular spheroids as a model for cell kinetic studies.* Cell Tissue Kinet. 23: 141–159 (1990).

[20] J. Folkman and M. Hochberg. *Self-regulation of growth in three dimensions.* J. Exp.Med. 138: 745–753 (1973).

[21] J.P. Freyer. *Role of necrosis in regulating the growth saturation of multicellular spheroids.* Cancer Res. 48(9): 2432–2439 (1988).

[22] C. Giverso and P. Ciarletta. *On the morphological stability of multicellular tumour spheroids growing in porous media.* Eur. Phys. J. E 39(10): 92 (2016).

[23] C. Giverso and L. Preziosi. *Modelling the compression and reorganization of cell aggregates.* Math. Med. Biol. 29 (2): 181–204 (2012).

[24] C. Giverso and L. Preziosi. *Behavior of cell aggregates under force-controlled compression.* Int. J. Non-Linear Mech. 56: 50–55 (2013).

[25] H.P. Greenspan. *On the growth and stability of cell cultures and solid tumours.* J. Theor. Biol. 56: 229–242 (1976).

[26] A. Grillo, A., S. Federico, G. Wittum. *Growth, mass transfer, and remodeling in fiber-reinforced, multi-constituent materials.* Int. J. Non-Linear Mech. 47: 388–401 (2012).

[27] A. Grillo, C. Giverso, M. Favino, R. Krause, M. Lampe, G. Wittum. *Mass transport in porous media with variable mass.* Numerical Analysis of Heat and Mass Transfer in Porous Media. A. Oechsner, L.F.M. da Silva, H. Altenbach Eds. Springer Verlag Germany (2012).

[28] D.R. Grimes, C. Kelly, K. Bloch and M. Partridge. *A method for estimating the oxygen consumption rate in multicellular tumour spheroids.* J. R. Soc. Interface 11 (92): 20131124 (2014).

[29] K. Groeber, W. Mueller-Klieser. *Distributions of oxygen, nutrient and metabolic waste concentrations in multicellular spheroids and their dependence on spheroid parameters.* Eur. Biophys. J., 19: 169–181 (1991).

[30] G. Hamilton. *Multicellular spheroids as an in vitro tumour model.* Cancer Lett. 131: 29–34 (1998).

[31] M.H. Holmes and V. C. Mow. *The nonlinear characteristics of soft gels and hydrated connective tissues in ultrafiltration.* J. Biomech. 23(11): 1145–1156 (1990).

[32] J. Humphrey and K. Rajagopal. *A constrained mixture model for growth and remodeling of soft tissues.* Math. Mod. Meth. Appl. Sci. 22: 407–430 (2002).

[33] J. Humphrey and K. Rajagopal. *A constrained mixture model for arterial adaptations to a sustained step change in blood flow.* Biomech. Model. Mechanobiol. 2: 109–126 (2003).

[34] J.F.R. Kerr, C.M. Winterford and B.V Harmon. *Apoptosis. Its significance in cancer and cancer therapy.* Cancer 73(8): 2013–2026 (1994).

[35] D.V. Krysko, T.V. Berghe, K. D'Herde and P. Vandenabeele. *Apoptosis and necrosis: detection, discrimination and phagocytosis.* Methods 44(3): 205–221 (2008).

[36] V. Kumar, A.K. Abbas, J.C. Aster and N. Fausto. *Pathologic basis of disease*, 8 Edn. Chap. 1. Saunders Elsevier, Philadelphia, PA USA (2009).

[37] L.A. Kunz-Schughart, M. Kreutz and R. Knuechel. *Multicellular spheroids: a three-dimensional in vitro culture system to study tumour biology.* Int. J. Exp. Path. 79: 1–23 (1998)

[38] G. Landini and J.W. Rippin. *How important is tumour shape?* J. Pathol. 179: 210–217 (1996).

[39] E.H. Lee. *Elastic-plastic deformation at finite strains.* ASME Transaction on J. Appl. Mech. 36: 1-6 (1969).

[40] J.S. Lowengrub, H.B Frieboes, F. Jin, Y.L Chuang, X. Li, P. Macklin, S.M. Wise and V. Cristini. *Nonlinear modelling of cancer: bridging the gap between cells and tumours.* Nonlinearity 23: R1–R91 (2010).

[41] P. Macklin, S. Mumenthaler and J. Lowengrub. *Modeling multiscale necrotic and calcified tissue biomechanics in cancer patients: application to ductal carcinoma in situ (DCIS).* In: Gefen A. (eds) Multiscale Computer Modeling in Biomechanics and Biomedical Engineering. Studies in Mechanobiology, Tissue Engineering and Biomaterials, vol 14. Springer, Berlin, Heidelberg (2013).

[42] P. Mascheroni, D. Boso, L. Preziosi and B.A. Schrefler. *Evaluating the influence of mechanical stress on anticancer treatments through a multiphase porous media model.* J. Theor. Biol. 421: 179–188 (2017).

[43] P. Mascheroni, M. Carfagna, A. Grillo, D.P. Boso and B.A. Schrefler. *An avascular tumor growth model based on porous media mechanics and evolving natural states.* Math. Mech. Solids 23(4): 686–712 (2018).

[44] W. Mueller-Klieser. *Multicellular spheroids: a review on cellular aggregates in cancer research.* J. Cancer Res. Clin. Oncol. 113: 101–122 (1987).

[45] E. Noch and K. Khalili. *Molecular mechanisms of necrosis in glioblastoma: the role of glutamate excitotoxicity.* Cancer Biol. Ther. 8(19): 1791–1797 (2009).

[46] F.P. O'Malley. *Lobular neoplasia: morphology, biological potential and management in core biopsies.* Mod. Pathol. 23: S14–S25 (2010).

[47] C.P. Please, G.J. Pettet and D.L.S. McElwain. *A new approach to modelling the formation of necrotic regions in tumours.* Appl. Math. Lett. 11: 89–94 (1998).

[48] C.P. Please, G.J. Pettet and D.L.S. McElwain. *Avascular tumour dynamics and necrosis.* Math. Models Methods Appl. Sci. 9: 569–579 (1999).

[49] L. Preziosi and A. Tosin. *Multiphase and multiscale trends in cancer modelling.* Math. Model. Nat. Phenom. 4: 1–11 (2009).

[50] L. Preziosi, D. Ambrosi and C. Verdier. *An elasto-visco-plastic model of cell aggregates.* J. Theor. Biol. 262: 35–47 (2010).

[51] K.R. Rajagopal and A. R. Srinivasa. *On the thermomechanics of materials that have multiple natural configurations Part I: viscoelasticity and classical plasticity.* Z. angew. Math. Phys. 55: 861–893 (2004).

[52] A. Raza, H.E. Colley, El. Baggaley, I.V. Sazanovich, N.H. Green, J.A. Weinstein, S.W. Botchway, S. MacNeil and J.W. Haycock, *Oxygen mapping of melanoma spheroids using small molecule platinum probe and phosphorescence lifetime imaging microscopy.* Sci. Rep. 7: 10743 (2017)

[53] C.H. Richards, C.S.D. Roxburgh, J.H. Anderson, R.F. McKee, A.K. Foulis, P.G. Horgan and D.C McMillan. *Prognostic value of tumour necrosis and host inflammatory responses in colorectal cancer.* Brit. J. Surg. 99(2): 287–294 (2012).

[54] E.K. Rodriguez, A. Hoger and A. McCulloch. *Stress-dependent finite growth in soft elastic tissues.* J. Biomech. 27: 455–467 (1994).

[55] G. Sciumè, S. Shelton, W.G. Gray, C.T Miller, F. Hussain, M. Ferrari, P. Decuzzi and B.A Schrefler. *A multiphase model for three-dimensional tumor growth.* New J. Phys. 15: 015005 (2013).

[56] M.D. Sherar, N.B. Noss and F.S. Foster. *Ultrasound backscatter microscopy images the internal structure of living tumour spheroids.* Nature 330: 493–495 (1987).

[57] J.A. Sherratt and M.A. Chaplain. *A new mathematical model for avascular tumour growth.* J. Math. Biol. 43: 291–312 (2001)

[58] A.R. Skovoroda, A.N. Klishko, D.A. Gusakyan, Y.I. Mayevskii, V.D. Yermilova, G.A. Oranskaya and A.P. Sarvazyan. *Quantitative analysis of the mechanical characteristics of pathologically changed soft biological tissues.* Biophysics 40: 1359–1995 (1995).

[59] R.M. Sutherland, J.A. McCredie and W.R. Inch. *Growth of multicell spheroids in tissue culture as a model of nodular carcinomas.* J. Natl. Cancer Inst. 46: 113–120 (1971)

[60] R.M. Sutherland. *Cell and environment interactions in tumour microregions: the multicell spheroid model.* Science 240: 177–184 (1988).

[61] R.M. Sutherland, R.E. Durand. *Growth and cellular characteristics of multicell spheroids.* Recent Results Cancer Res. 95: 24–49 (1984).

[62] R.H. Thomlinson and L.H. Gray.*Histological structure of some human lung cancers and the possible implications for radiotherapy.* Brit. J. Cancer. 9: 539–549 (1955).

[63] P. Tracqui. *Biophysical models of tumour growth.* Rep. Prog. Phys. 72: 056701 (2009).

[64] C. Verdier, J. Etienen, A. Duperray and L. Preziosi. *Review: rheological properties of biological materials.* Compt. Rend. Physics 10(8): 790–811 (2009).

[65] D.I. Wallace and X. Guo. *Properties of tumor spheroid growth exhibited by simple mathematical models.* Front. Oncol. 3: 51 (2013).

[66] E. Wibe, T. Lindmo and O. Kaalhus. *Cell kinetic characteristics in different parts of multicellular spheroids of human origin.* Cell Tissue Kinet. 14: 639–651 (1981).

[67] S.M. Wise, J.S. Lowengrub, H.B. Frieboes and V. Cristini. *Three-dimensional multispecies nonlinear tumor growth: I. Model and numerical method* J. Theor. Biol. 253 524–543 (2008)

[68] H. Yagata, K. Harigaya, M. Suzuki, T. Nagashima, H. Hashimoto, G. Ishii, M. Miyazaki, N. Nakajima and A. Mikata. *Comedonecrosis is an unfavorable marker in node-negative invasive breast carcinoma.* Pathol. Int. 53(8): 501–506 (2003).